Journal of Power Sources 196 (2011) 8129–8139

Contents lists available at ScienceDirect

Journal of Power Sources

journal homepage: www.elsevier.com/locate/jpowsour

Modeling stresses in the separator of a pouch lithium-ion cell

Danghe Shi [a], Xinran Xiao [a,*], Xiaosong Huang [b], Hamid Kia [b]

[a] Mechanical Engineering, Michigan State University, 2727 Alliance Dr, Lansing, MI 48910, United States
[b] Chemical Sciences & Materials Systems Lab, General Motors Global R & D, 30500 Mound Rd, Warren, MI 48090, United States

ARTICLE INFO

Article history:
Received 22 February 2011
Received in revised form 6 May 2011
Accepted 12 May 2011
Available online 20 May 2011

Keywords:
Separator
Lithium-ion battery
Intercalation stress
Thermal stress

ABSTRACT

The stress in a separator is mainly caused by the lithium diffusion induced deformation in the electrodes and thermal expansion differential between the battery components. To compute the lithium concentration distribution and temperature change during battery operation, multi-physics models have been developed previously. In this work, a macro-scale model for a pouch cell was developed and coupled with the multi-physics models. In this model, the porous battery components were treated as homogenized media and represented with the effective properties estimated using the rule of mixtures. The stress analysis showed that the maximum stress in the separator always emerged at the area around the inner corner of the separator where it wrapped around the edge of an anode and when the lithium-ion battery was fully charged. Numerical simulations were also conducted to investigate the influences of some design adjustable parameters, including the effective friction, electrode particle radii and thickness of the separator, on the stresses in the separator. The results provided the reference conditions for the improvement of separator materials and the design of lithium-ion batteries.

1. Introduction

Lithium-ion batteries offer high specific energy, high energy density and low self-discharge rate, and thus have been widely used in consumer electronics. Lithium-ion technology is also the primary choice in the current electric vehicles (EVs), hybrid vehicles (HEVs), and plug-in hybrid vehicles (PHEVs). Nevertheless, significant material and processing technological barriers still exist, mainly in cost, performance, abuse tolerance, and durability. These issues, especially those related to abuse tolerance, become more severe as the cell sizes increase in order to meet the power requirement for vehicle propulsion [1]. Short circuits due to separator failure, battery over-charge and over-discharge, and high temperature can lead to a thermal event [2]. To prevent separator failure, one must fully understand the functionality of a separator and its working environment in a battery.

In a lithium-ion battery, in addition to the stresses introduced in cell assembly process and the mechanical load on the battery pack, the separator is subjected to the stresses induced by the intercalation deformation of the electrodes and thermal expansion differential between the battery components. There is no method to measure the stresses in the separator *in situ* in a battery.

The objective of this research is to develop a numerical model for the stress analysis of the separator in a realistic battery cell. To compute the stresses from various sources, all relevant physical phenomena have to be included. The current work is based on battery kinetics [3,4], intercalation stress [5–14] and thermal [15–18] models that have been developed in the past.

Newman and his co-workers have developed a series of models for lithium-ion batteries. Today, most of the modeling works on the kinetics of lithium-ion batteries are based on a 1D model presented by Doyle et al. [3,4]. In this model, each porous electrode was treated as a pseudo homogeneous mixture of the solid active material and the electrolyte. The model predictions were in good agreement with the experimental results.

In recent years, with the discoveries of new, high capacity electrode materials, the intercalation induced stresses in the electrode particles has become a hot topic. Christensen and Newman studied the stress generated inside the $Li_yMn_2O_4$ [5] and carbon [6] electrodes. Zhang et al. [7] considered the stress effect on lithium diffusion and the stress distribution inside one single electrode particle using numerical simulation. Cheng and Verbrugge compared the stress evolution process under the galvanostatic and potentiostatic operation [8], and studied the effects of surface tension and modulus on the diffusion induced stress within spherical nano-particles [9]. Verbrugge and Cheng [10] also examined the stress in spherical particles under periodic potential excitations. Renganathan et al. [11] considered the stress arising due to the phase transformation in their model. Golmon et al. [12] presented a multi-scale finite element approach to study the electrochemical–mechanical interaction phenomena at macro-, meso-, and micro-scales.

* Corresponding author. Tel.: +1 517 884 1606; fax: +1 517 884 1601.
E-mail address: xinran@msu.edu (X. Xiao).

0378-7753/$ – see front matter © 2011 Elsevier B.V. All rights reserved.
doi:10.1016/j.jpowsour.2011.05.026

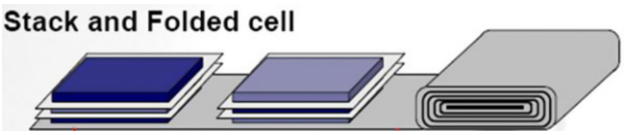

Fig. 1. Schematic of a pouch cell [20].

Although most of the stress analysis was limited to one single particle, 2D models have appeared in literature. Garcia et al. [13] developed a 2D model to study the effects of size and size distribution of the cathode particles. This model, however, did not consider the real contact between different battery components and the real boundary conditions. Xiao et al. [14] developed a multi-physics, multi-scale model of a lithium-ion battery cell using COMSOL, which considered the reaction kinetics, lithium diffusion, and diffusion induced stress. However, the contact algorithm in the multi-physics code was not robust enough and a continuous mesh had to be used across the components. The stress calculated by this approach may only represent the condition in the center of a cell.

As for the thermal behavior of a lithium-ion battery, although several studies have addressed the issue of heat generation inside lithium-ion batteries, most works were conducted to describe the heat generation, temperature change, or their influence on certain electrochemical properties [15–18]. Few researches have considered the thermally induced stress. As an extension of Xiao's work, Wu et al. [19] introduced thermal stress in a 2D lithium-ion battery model. The results showed that, for the separator, the influence of the thermal stress was as significant as that of the lithium diffusion induced stress.

This paper presents a stress analysis for a separator in a pouch lithium-ion battery cell. A pouch cell is manufactured by stacking up layers of electrodes and separator films as showed schematically in Fig. 1 [20]. In this work, the pouch cell was represented by a macro-scale 2D plane strain model. The stress analysis was performed using a structural analysis package ANSYS.

Limited by the availability of the data and understanding on the multi-physics processes in lithium-ion batteries, at this stage of the work, all materials were assumed to be linear elastic and isotropic, all the material properties were considered to be independent of lithium concentration and temperature.

2. Separator

2.1. About separators

In a battery, the separators are sandwiched between positive and negative electrodes and then spirally packed together in cylindrical or folded back and forth in prismatic configurations. The pores of the separators are filled with some ionically conductive liquid electrolyte [21]. Separators are intended to prevent electronic contact and enable ionic transport between the positive and negative electrodes. In order to accomplish these functions, separators must be chemically and electrochemically stable towards the electrolyte and electrodes and mechanically strong to withstand the high tension during the battery assembly and cyclic stresses in charge–discharge cycles during its life time [21–24].

The battery separators can be broadly divided into three categories: porous polymer membranes, non-woven fabric mats, and inorganic composite membranes [21]. They are featured by the thinness, high porosity, and excellent thermal stability, respectively. Among them, the porous polyolefin membranes have been most widely used in liquid electrolyte batteries due to their comprehensive advantages in performance and cost [1,23,24].

Porous polymeric separators have been developed from simple porous films to complex multilayer structures in order to meet the increasing demands of high-energy batteries. The thin layers (<30 μm) are made of polyethylene (PE), polypropylene (PP), or laminates of these two. PE and PP are low cost polyolefin materials, which offer excellent chemical stability and good mechanical properties [21].

2.2. Stress sources in separators

Besides the residual stress induced in the cell assembly process and mechanical load on the battery pack, additional stresses may arise in the separator during charge–discharge operation. Two sources of stresses have been identified [14], one is due to the deformation of the electrodes and the other is due to thermal expansion differential between components.

For a typical $Li_yMn_2O_4$ cathode and a carbon anode, the chemical reactions for cell charging are shown as [25]:

Anode:

$$xLi^+ + C_6 + xe^- \rightarrow Li_xC_6$$

Cathode:

$$Li_yMn_2O_4 \rightarrow xLi^+ + xe^- + Li_{y-x}Mn_2O_4$$

This moving mechanism is primarily based on the diffusion processes: deliver lithium ions to the surface of the cathode, transfer to and diffuse in the electrolyte through the separator, and then transfer to and diffuse into the anode [2]. The discharging process proceeds in the opposite direction. The intercalation and deintercalation processes result in volume changes in the active electrode materials, and thus the entire electrode. In a tightly packed battery, the fluctuations in the electrode sizes cause the separator to deform and hence stresses.

The heat generation accompanied with electrochemical reactions in a battery can be significant. The environmental temperature also fluctuates. The difference in the expansion rates of different battery components induces thermal stress in the separator.

3. Modeling methods

3.1. Depiction of multiphysical phenomena

The phenomena occurring inside a lithium-ion battery can be generally classified into three groups: electrochemical, thermal, and mechanical phenomena. Each group is described by a different set of equations. Since they are strongly related to each other, they will be investigated as coupled phenomena in order to accurately and systematically analyze the stresses.

The electrochemical reactions serve as the foundation for all these analysis. Detailed mathematical models have already been established by Doyle et al. [3,4]. In the current study, the analysis of electrochemical phenomena was built upon these well established mathematical models.

According to Wu et al. [19], the thermal stress imposed on the separator due to the self-heating of the battery is substantial. To understand the stress behavior of a lithium-ion battery, the self-heating of the battery must be considered.

The general heat transfer equation is given by [17]:

$$\rho_i C_{p\_i} \frac{\partial T}{\partial t} = \nabla \cdot (\lambda_i \ \nabla T) + q_i \quad (1)$$

where from left to right, the terms denote heat accumulation, heat conduction, and heat generation. $i = a$ or c, where a represents anode and c represents cathode.

The heat generation in a lithium-ion battery was considered based on the framework derived by Bernadi et al. [15] based on

the energy balance of the battery system. There are mainly four sources [17,19], which can be written as

$$q_i = s_{a\_i} j_{n\_i}(\phi_1 - \phi_2 - U_i) + s_{a\_i} j_{n\_i} T \frac{\partial U_i}{\partial T} + \sum_k \Delta H_k^{avg} r_k + \int \sum_r \sum_s (\bar{H}_{rs} - H_{rs}^{avg}) \frac{\partial c_{rs}}{\partial t} dv \quad (2)$$

where s_{a_i} is the specific surface area ($m^2\ m^{-3}$) and j_{n_i} is the current density ($A\ m^{-2}$). In Eq. (2), the first term is the irreversible resistive heat, representing the deviation of the cell potential from its equilibrium value; the second term is the reversible entropy heat; the third term is the chemical side reaction heat; and the fourth term is the heat of mixing due to the generation and relaxation of concentration gradients. As revealed in Ref. [18], the heat of mixing is relatively small compared to entropic and resistive heat, thus it can be neglected. In this study, a binary electrolyte is assumed and side reactions and phase change effects are neglected. The energy balance equation reduced to

$$\rho_i C_{p\_i} \frac{\partial T}{\partial t} = \nabla \cdot (\lambda_i \nabla T) + s_{a\_i} j_{n\_i}(\phi_1 - \phi_2 - U_i) + s_{a\_i} j_{n\_i} T \frac{\partial U_i}{\partial T} \quad (3)$$

Experimental results of $\partial U/\partial T$ for $LiMn_2O_4$ [26] and LiC_6 [27,28] are used in this study.

For mechanical phenomena, a linear elastic behavior was assumed and Young's modulus was treated as a constant in this work. Besides the mechanical (elastic) strain, the thermal strain [19] and diffusion induced strain also arise in lithium-ion batteries [7,14]. The constitutive relationship can be written as

$$\varepsilon_{ij} = \varepsilon_{ij}^{me} + \varepsilon_{ij}^{ei\_T} + \varepsilon_{ij}^{ei\_c} = \frac{1}{E}((1+\nu)\sigma_{ij} - \nu\sigma_{kk}\delta_{ij}) + \alpha_{ij}\ \Delta T\delta_{ij} + \frac{1}{3}\Delta c \Omega \delta_{ij} \quad (4)$$

where ε_{ij} is the strain component, E is Young's modulus, ν is the Poisson's ratio, σ_{ij} is the stress component, δ_{ij} is the Kronecker delta, α_{ij} is thermal expansion coefficient, ΔT is the temperature change from the reference value, Δc is the concentration change of diffusion species from the reference value, and Ω is the partial molar volume. Ω has a unit of $m^3\ mol^{-1}$, which is the volume expansion per mole of insertion species in the host material. Ω can be treated as a coefficient analogous to the thermal expansion coefficient. For isotropic volume expansion [16]:

$$\Omega = \frac{3\varepsilon}{\Delta y c_{max}} \quad (5)$$

where ε is the intercalation induced strain along the major axis of the material, Δy is the change of the number of lithium atoms, and c_{max} is the stoichiometric maximum concentration.

3.2. Multi-physics coupling

There are mainly two sources of stress in a separator associated with the operation of the battery: lithium diffusion induced stress and thermal stress. The lithium and temperature distributions, therefore, are needed in stress analysis. This was realized by a set of models as illustrated in Fig. 2.

Fig. 2 shows three models: a pseudo 2D battery model at the top panel; a macro-scale 2D model at bottom to the left and a 1D cross section model to the right. The final stress analysis was performed in the macro-scale 2D model and the other two models worked as assistant models.

The pseudo 2D battery model consists of a 1D porous electrode model and a 2D spherical particle model. This model is available in COMSOL 3.5a [29], which was built upon the model developed by Doyle et al. [3,4]. The 1D porous electrode model considers the electronic current balance, ionic charge balance, material balance, and electrochemical interface kinetics, while the 2D spherical particle model provides the lithium concentration distribution in the active particles for the 1D porous electrode model.

A previous study by Xiao et al. [14] has showed that the stress inside the separator changed little while lithium concentration profiles inside the electrode relaxed during a 1000s open circuit period in a charge–discharge cycle. In other words, the redistribution of lithium ions inside the electrodes had negligible effect on the stress inside the separator. Based on this finding, to simplify the model, lithium ions inside each particle were assumed to be evenly distributed. As the result, the lithium concentration profile only varied along the thickness direction of the electrodes.

The distribution of lithium ions in the thickness direction was obtained by projecting the distribution of the 2D spherical particle model onto the 1D cross section model. Each point of the 1D cross section model represents an averaged value of lithium concentra-

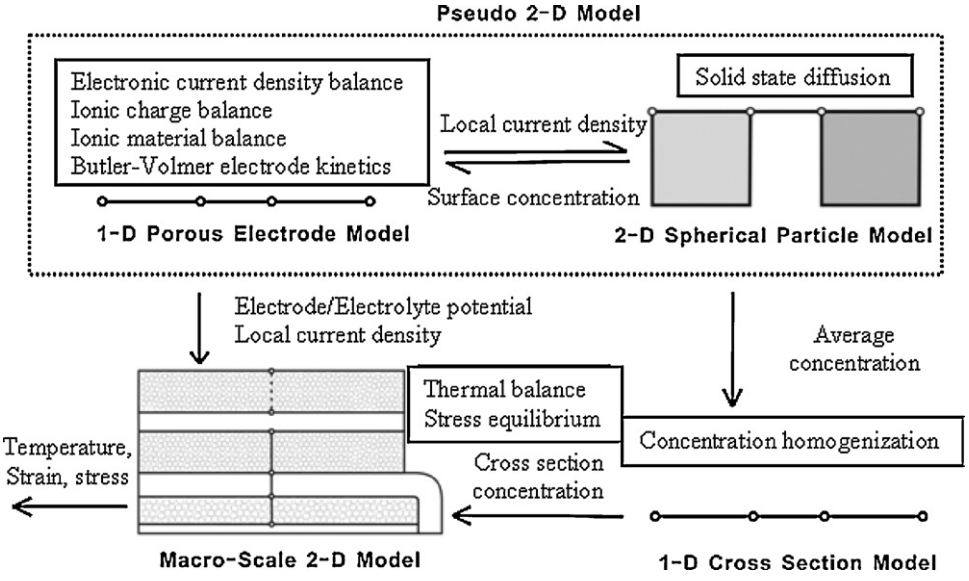

Fig. 2. Schematic of multi-physics coupling methods used in this work. The pseudo 2D battery models were used to simulate electrochemical reactions. The 1D cross section model was used to couple the macro-scale 2D model with the pseudo 2D models. Both thermal and stress analysis were performed in the macro-scale 2D model.

tion in a sphere particle of radius R derived from the 2D spherical particle model. The average lithium concentration inside a particle, C_{ave}, was calculated by

$$c_{ave} = \frac{1}{(4/3)\pi R^3}\int_0^R 4\pi r^2 c_1 dr = \frac{3}{R^3}\int_0^R r^2 c_1 dr \quad (6)$$

In the 2D spherical particle model, a normalized radius distance was used such that $y = r/R$, $y \in [0, 1]$, the equation can be rewritten as

$$c_{eff\_i} = 3\int_0^1 c_1 y^2 dy \quad (7)$$

where c_{eff_i} is the average concentration of lithium in the ith electrode particle in the 1D cross section model, c_1 is the concentration of lithium along the radius in the 2D spherical particle model. The through thickness distribution of lithium concentration at each electrode obtained from Eq. (7) was then projected to the macro-scale 2D model.

The thermal analysis was performed on the macro-scale 2D model using COMSOL. As presented in Eq. (3), in addition to the lithium ion concentration, some other variables such as current density and potential are needed for the calculation of heat generation. These variables were directly projected from the 1D porous electrode model.

Inputting the above extracted distributions into the macro-scale 2D model, the stress analysis of the battery could be performed subsequently.

4. Macro-scale model

As introduced before, each cell is composed of parallel layers of different components. The stress in the middle part of the pouch battery may converge to a stable value, but the stress at the battery edges can vary greatly depending upon the separator wrapping method and the actual geometry of the edges of the electrodes.

There are two ways to wrap the separator around the electrodes during assembly: wrap around the anode and/or wrap around the cathode. In this work, all the transported lithium ions were assumed to come from the cathode. Under this condition, in one charge–discharge cycle, deformation induced by lithium diffusion causes the cathode to shrink and then expand back to its original dimensions. The deformation of the anode proceeds in an opposite manner. Therefore, only the separator wrapped around the anode is expected to experience high strain and stress fluctuations. The thermal expansion under these conditions would reduce the stress and strain regardless of the wrapping method. In order to determine the maximum stress imposed on the separator, only the case of wrapping the separator around an anode was considered.

The shape of the electrode edge may change according to different assembly methods. For the model in this research, the separator was assumed to wrap tightly around the anode and the transition area (edge) was considered to be annulus. The maximum stress yields from this model can be considered as the lower bound when compared to other possible conditions.

4.1. Model depiction

The macro-scale 2D model is shown in Fig. 3. The model is regularly shaped with smooth surfaces. A Cu/Li_yC_6/PP/$Li_yMn_2O_4$/Al cell has been selected in this research. The components from the bottom to the top are anode current collector (Cu), anode, separator, cathode 1, cathode current collector (Al), and cathode 2. The separator is wrapped around the anode and assembled tightly with the anode and cathode. It is important to note that a 1.5 cell model was built in this study instead of a full cell. If a full cell were modeled,

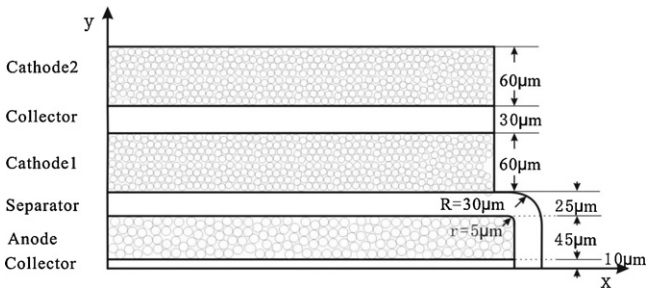

Fig. 3. Schematic of the structure of the model.

one layer of cathode and one layer of collector would form an asymmetric beam which tends to bend under diffusion induced stress in the cathode layer so to separate away from the separator. In most cases, since the collector is coated with cathode layers on both sides, the bending forces will always be counteracted by each other. To represent this common situation, one needs to add another cathode layer into the full cell model, and therefore a 1.5 cell model was formed. The collector for the anode is coated at both sides as well. This was represented by a symmetrical boundary condition at the lower surface of the current collector in the model.

Fig. 4 presents the schematic of the mechanical boundary conditions of the macro-scale 2D model. There are two groups of boundaries in this model: external and internal. To set the boundary conditions, one needs to consider the production process of battery cells. At the beginning of the production process, a cathode paste is spread on an Al foil (cathode current collector) and an anode paste is spread on a Cu foil (anode current collector), and therefore the electrodes and their corresponding collectors are always bonded together. These bonded components are then wrapped sequentially with separators [30]. Relative slip can occur on the interfaces between a separator and its adjacent electrodes. Due to this production process, for the internal boundaries, a contact relationship was assigned at the boundaries between the separator and electrodes in the model; and the boundaries between the electrodes and the corresponding current collectors were modeled as continuous. For the external boundaries, the prismatic pouch cells have a flexible, foil-type case. Distributed normal pressure was assigned to the top boundary. The default value for this pressure was 10 psi. A symmetric displacement boundary condition was assigned to the left and bottom boundaries. The rest of the external boundaries were free boundaries.

As to the thermal boundary conditions, a convective boundary condition with a coefficient of $H = 5\,W\,m^{-2}\,K^{-1}$, corresponding to the case in air, was assigned to the right and up side boundaries. For all other sides, an adiabatic boundary condition was applied because of the symmetric conditions. Inside the lithium-ion battery, heat can be conducted freely from one component to another;

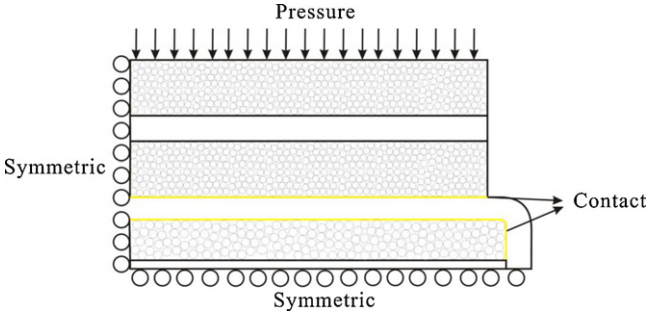

Fig. 4. Schematic of mechanical boundary conditions for the real 2D model.

therefore, free conductive boundary conditions were applied for all the inner boundaries.

4.2. Effective material properties

The separator and electrodes are porous and filled with electrolytes. In this research, all components were modeled as a homogeneous solid medium. The material porosity was taken into consideration through the use of effective properties. This study was focused on the stress in the separator. It was assumed that, when observed macroscopically, the local details of the electrodes would not constitute a significant influence on the stress in the separator. In other words, the same macroscopic behavior can be obtained with the effective properties of a homogenized medium, as long as the equivalent macroscopic strains of the electrodes are generated.

4.2.1. Diffusion and thermal induced expansion coefficients

A porous solid filled with electrolyte can be treated as a composite of the solid material and electrolyte. In this study the electrolyte was considered to be compressible, but its volume variation due to Li^+ concentration change was assumed to be negligible. In electrodes, only the active particles experienced lithium diffusion induced volume change. To account for this influence, an effective diffusion expansion coefficient was estimated by the rule of mixtures similar to composite systems as [31]:

$$\beta_{eff} = \sum_i \beta_i V_i = \sum_i \frac{1}{3}\Omega_i V_i \tag{8}$$

where β_{eff} is the effective diffusion expansion coefficient of the composite and β_i and V_i are the diffusion induced expansion coefficient and the volume fraction of the ith phase, respectively. Neglecting the contribution of the electrolyte phase, the expression can be reduced to

$$\beta_{eff} = \beta_p V_p = \frac{1}{3}\Omega_p V_p \tag{9}$$

where β_p and V_p are the diffusion induced expansion coefficient and the volume fraction of the active particles, respectively. With this effective diffusion expansion coefficient, the macroscopic equivalent strain of an electrode due to lithium insertion and extraction can be obtained.

The effective thermal expansion coefficient of the electrode was estimated in the same way, but the expansion of the electrolyte cannot be neglected. The effective thermal expansion coefficient is defined as:

$$\alpha_{eff} = \sum_i \alpha_i V_i \tag{10}$$

where α_{eff} is the effective thermal expansion coefficient of the composite and α_i is the diffusion induced expansion coefficient of the ith phase.

4.3. Thermal conductivities and specific heat capacities

The method used to obtain the effective thermal conductivity and specific heat capacity was very similar to the one for expansion coefficients. For 1D problem, the effective thermal conductivity is calculated by $k_{eff}\sum_i L_i = \sum_i k_i L_i$ [31], where k_{eff} is the effective thermal conductivity of the composite, k_i is the thermal conductivity of the ith phase, L_i represents the length of ith component. In a 3D space, L_i is replaced by an effective length $L_i \approx \sqrt[3]{V_i}$ and hence

$$k_{eff} = \frac{\sum_i k_i L_i}{\sum_i L_i} \approx \frac{\sum_i k_i \sqrt[3]{V_i}}{\sum_i \sqrt[3]{V_i}} \tag{11}$$

The effective specific heat capacities were calculated by [31]:

$$c_{p\_eff} = \frac{\sum_i c_{p\_i} m_i}{\sum_i m_i} = \frac{\sum_i c_{p\_i}\rho_i V_i}{\sum_i \rho_i V_i} \tag{12}$$

where c_{p_eff} is the effective specific heat capacity of the composite, c_{p_i} is the specific heat capacity of the ith phase, m_i is the mass fraction of ith phase, and ρ_i is the density of the ith phase.

4.3.1. Young's modulus

Similarly, Young's modulus of a porous electrode is different from that of an electrode particle. The effective modulus of a composite consisting of particles dispersed in a matrix was found to fall between the following upper and lower bounds, respectively [31,32]:

$$\text{Upper bound}: E_{eff} = E_m V_m + E_p V_p \tag{13}$$

$$\text{Lower bound}: E_{eff} = \frac{E_m E_p}{V_m E_p + V_p E_m} \tag{14}$$

where E_{eff} is the effective Young's modulus of the composite, and E_m and E_p are Young's moduli of the matrix and particles, respectively.

In this work, the mass fraction of the active materials in electrodes was assumed to be 0.8 [33]. From the mass fraction and densities of battery components, the computed volume fraction of the active materials was 0.69 for the carbon anode and 0.53 for the $LiMn_2O_4$ cathode. At a high particle volume fraction, the upper bound estimation provides a closer approximation [32] and, therefore, the upper bound prediction described by Eq. (13) was used to calculate the effective Young's modulus.

Table 1 provides a summary of the material constants reported in the literature [4,13,14,21,29,34] and the effective values computed using the rule of mixtures described in Eqs. (8)–(14) for different battery components.

5. Simulation

5.1. Simulation conditions

The strain and stress of a separator in a $Cu/Li_yC_6/PP/Li_yMn_2O_4/Al$ battery at the end of a charging period were investigated. The charging process consisted of two steps: charge the battery at constant current until reaching a voltage of 4.2 V, and then hold the cell voltage at 4.2 V while gradually reducing the charging current until it drops to a small percentage of the initial value, such as 3%. At this point, the battery is considered to be fully charged [35]. The stress free conditions were assumed to be those of the battery before the first charge.

In normal operation conditions, the concentration of Li^+ in electrodes is in the range of 0.2–0.9 in terms of the state of charge (SOC)—the ratio of local lithium concentration to stoichiometric maximum concentration. In this work, the battery initially was at a discharged state with a SOC = 0.2 for anode and SOC = 0.9 for cathode. During charging, the SOC increases in the anode and decreases in the cathode. The SOC distribution in an electrode is not uniform. Fig. 5 depicts the SOC distribution for each electrode along its thickness at the end of a charging period. This was obtained by charging a battery for 3400s.

Table 1
Material properties of different battery components used in simulations.

	Unit	Cu	Anode	Separator[a]	Cathode	Al	Electrolyte
Electrochemical constants							
Density	$kg\,m^{-3}$	8700	2223	900	4202	2700	1210
Stoichiometric maximum concentration	$mol\,m^{-3}$		2.64×10^4 [4]		2.29×10^4 [4]		
Initial concentration	$mol\,m^{-3}$		5000		20500		2000
Diffusion coefficient	$m^2\,s^{-1}$		3.9×10^{-14}		7.08×10^{-15}		
Partial molar volume	$m^3\,mol^{-1}$		4.17×10^{-6}		3.5×10^{-6}		
Effective partial molar volume	$m^3\,mol^{-1}$		2.88×10^{-6}		1.86×10^{-6}		
Porosity			0.26	0.42 [21]	0.407		
Active volume fraction			0.69		0.53		
Thermal constants							
Thermal expansion coefficient	K^{-1}	17×10^{-6}	4.06×10^{-6}	13.32×10^{-5}	8.62×10^{-6}	23.6×10^{-6}	12.4×10^{-6}
Effective Thermal expansion coefficient	K^{-1}		6.025×10^{-6}	82.46×10^{-6}	9.615×10^{-6}		
Specific heat capacity	$J\,kg^{-1}\,K^{-1}$	386	623	1883	672	897	1800
Effective specific heat capacity	$J\,kg^{-1}\,K^{-1}$		823		839[34]		
Thermal conductivity	$W\,m^{-1}\,K^{-1}$	398	6.5	2.16	6.2	237	0.099
Effective thermal conductivity	$W\,m^{-1}\,K^{-1}$		3.81		3.28		
Heat transfer coefficient of air	$W\,m^{-2}\,K^{-1}$	5					
Mechanical constants							
Young's modulus	GPa	117	12	0.5	10	70	1 MPa [13]
Effective Young's modulus*	GPa		8.88		5.93		
Poisson's ratio		0.35	0.3	0.35	0.3	0.34	0.25 [13]

[a] All the none-electrolyte parts are treated as solid particles.

5.2. Stress distribution in the separator

Cell models of different lengths were investigated. It was observed that the maximum stress always occurred at the end of the charging period, and was located at the inner surface of the separator where it wrapped around the corner of the anode. Meanwhile, a homogeneous stress field was observed in the major part of the separator, which was away from the right side boundary. Fig. 6 presents the Von Mises stress distribution across the cell at the end of charging. The Von Mises stress is defined as [36]:

$$\sigma = \frac{\sqrt{2}}{2}\left[(\sigma_1 - \sigma_2)^2 + (\sigma_2 - \sigma_3)^2 + (\sigma_3 - \sigma_1)^2\right]^{1/2} \quad (15)$$

where σ_1, σ_2 and σ_3 are the three principle stress components. In general, the Von Mises stress governs the yielding and flow behavior of an isotropic material under a three-dimensional state of stress.

Fig. 7 presents the strain contours obtained around the edge. When the strain was plotted in the x and y directions, the corresponding maximum values were found along the horizontal and vertical segments of the separator near the edge. When plotted in the 1st principle strain, the maximum value in the separator was found at the area in contact with the edge of the anode. As shown, the contour of the 1st principle strain of the separator followed the shape of the edge, and this can be a potential failure area.

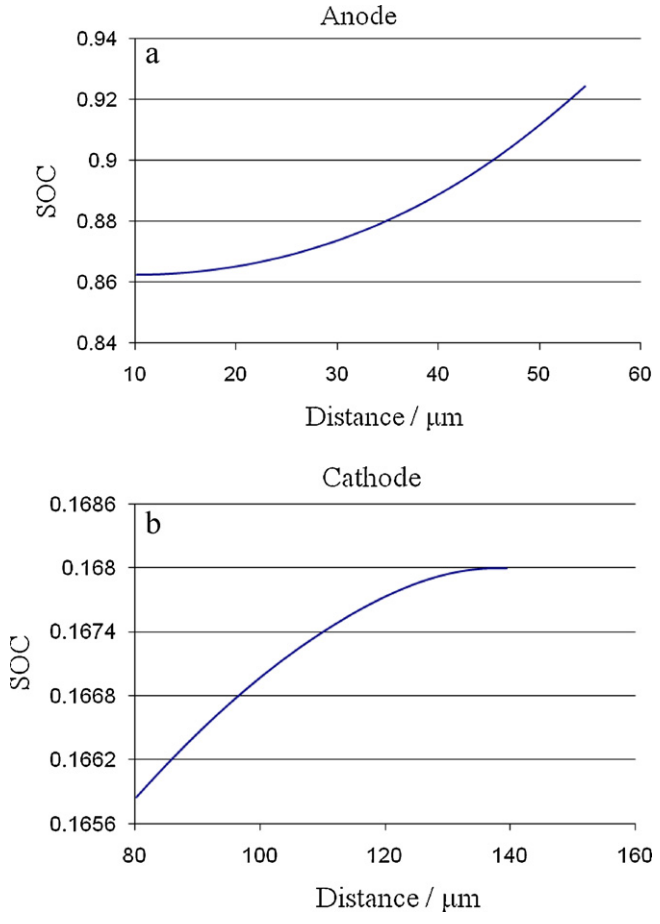

Fig. 5. Final SOC along the thickness of (a) anode and (b) cathode. The x coordinate distance denotes the y value in Fig. 3.

5.3. Thermal effect

For a battery in operation, temperature rise is an inevitable phenomenon. The thermal stress resulted from non-uniform thermal expansion can change the stress conditions in the separator significantly. The results showed that the temperature near the convective boundary was relatively low due to the direct convection with air. However, the gradient of the temperature field was

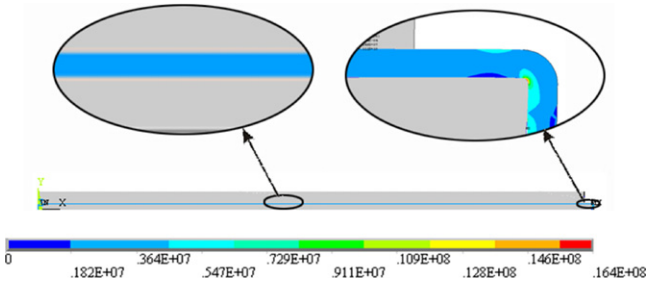

Fig. 6. Von Mises stress [Pa] in the separator. The maximum stress always located in the inner surface of the separator where it wrapped around the corner of the anode, while homogeneous stress fields were formed in the major part of the separator.

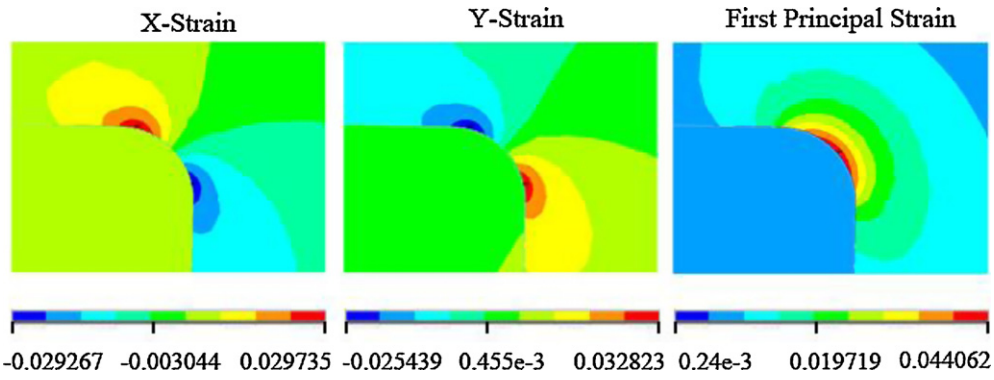

Fig. 7. Contours of strain [m m^{-1}] components in the separator near the corner.

Table 2
Comparisons of strain & stress in the separator with or without thermal effects.

	Average *x*-strain (%)	Average *y*-strain (%)	Maximum Von Mises stress (MPa)	Maximum 1st principal stress (MPa)
Without thermal effect	0.729	−0.40	27.2	17.8
With thermal effect	0.806	0.20	15.5	10.9

very small over the entire cell. This is due to the fact that the rate of heat conduction is much higher than the rate of heat generation and the cell is very thin. The temperature filed, therefore, can be treated as uniform [28].

The comparisons of the models with and without thermal effects are listed in Table 2. As expected, with the thermal effects, the total *x*-displacement of all battery components increased as a result of both mass diffusion expansion and thermal expansion. The corresponding average *x*-strain of the separator increased from 0.729% to 0.806%. The stress in the separator decreased dramatically after introducing thermal effects into the model. As shown in Fig. 8, the maximum Von Mises stress dropped 43% from 27.2 MPa to 15.5 MPa due to the differential in thermal expansions among the battery components. The results showed that, to represent the real working conditions of a battery, thermal effects need to be included.

It should be noted that the separator will begin to shrink when the temperature is higher than 90 °C. In this work, the maximum temperature was less than 60 °C and thus the unusual shrinkage of the separator was not considered. Furthermore, the material properties of battery components may vary with temperature. However, due to the complexity of the problem and lack of data, the material properties were treated as constants in most of the studies. In this work, all the numerical studies were conducted under the same temperature, thus, the influence of the thermal effect can be avoided when the effects of design adjustable parameters were discussed.

5.4. Effects of design adjustable parameters on stresses in the separator

Due to the linear assumptions, the current model cannot be used to perform failure analysis. However, it can be used to analyze the general influence trends of some design adjustable parameters on the stresses in the separator, and to improve the performance of the separator accordingly.

All lithium-ion batteries undergo a similar production process. However, there are some variations between batteries due to material selection and the shape of the battery components. A series of parameters were found to have a potential effect on the strain and stress conditions of a separator. These parameters include the porosity, interactive forces between the separator and electrodes, pressure, thickness of the separator, and electrode particle sizes [4,7,13]. Since these parameters can be adjusted in the design stage, thus they are named as design adjustable parameters. They can be generally classified into three groups: external parameters, internal parameters and manufacturing parameters as shown in Table 3.

In this work, only one parameter in each category was investigated. They are friction, electrode particle radius, and thickness of the separator.

5.4.1. Friction

The contact between the separator and electrodes may result in friction and viscous resistance. In the numerical models, a contact

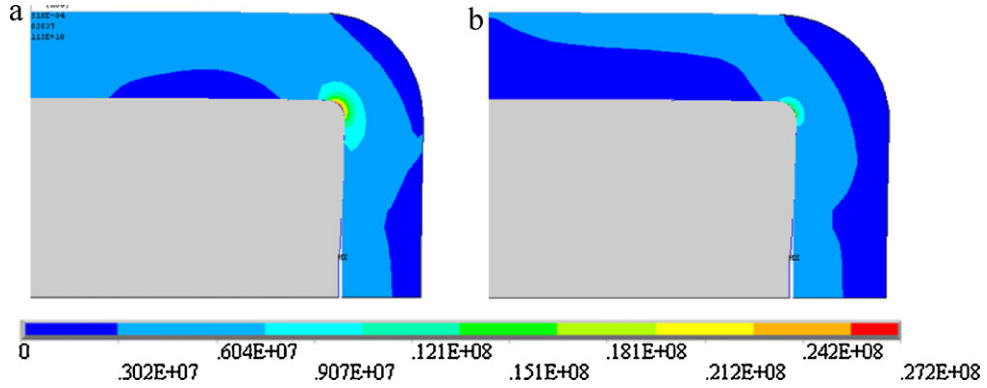

Fig. 8. Von Mises stress [Pa] in the separator (a) without and (b) with considering thermal effects in the whole battery field.

Table 3
Categories of design adjustable parameters.

Category	External parameters	Internal parameters	Manufacturing parameters
Parameters	Friction Pressure Temperature etc.	Particle radius Porosity Diffusivity etc.	Thickness Multiple separators Corner shape etc.

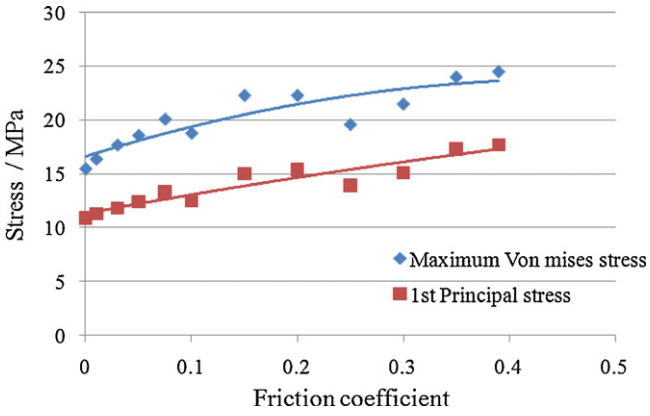

Fig. 9. Stresses versus effective friction coefficient.

relationship was defined and a corresponding effective friction was introduced for each pair of components in contact to simulate the effects of these interactions. Since the separator is relatively soft, the influence of the interactions between the separator and the electrodes can be significant. In this work, simulations were conducted with different effective friction coefficients ranging from 0.0 to 0.4.

As shown in Fig. 9, the influence of friction was significant. Generally an increase in the effective friction coefficient resulted in a greater maximum stress evaluated by both Von Mises stress and the 1st principal stress. This can be explained by the fact that, in order to generate a certain degree of deformation, the separator needs to overcome the resistance from itself as well as the surrounding components. Since the resistance from the surrounding components increases with friction, to generate the same amount of overall deformation, the local deformation of the separator (where friction occurs) will need to increase to counteract it.

The friction coefficient not only affects the magnitude, but also the location of the maximum stress, as shown in Fig. 10. As a higher friction coefficient caused the maximum stress to increase, the high stress area in the separator gradually shifted from the center to the upside of the edge. This phenomenon can be explained by the fact that the anode had a much larger contact area with the upper side than the right side of the separator. When friction was introduced, the relative displacement between the separator and the anode was restricted. The larger contact area at the upper side of the anode resulted in a larger friction force as compared to its right side. This increased the magnitude of the maximum tensile stress in the separator and moved the location of stress concentration. It is also the reason that the stress values obtained by numerical simulations fluctuated around the trend lines in Fig. 9.

In the stable stress area in the separator away from the right side boundary, the Von Mises stress value dropped slightly from 2.71 MPa to 2.62 MPa upon introducing friction. Further increases in the value of the friction coefficient, however, had no further effect on the Von Mises stress, as shown in Fig. 11.

From the above results, it can be concluded that friction can only affect the separator near the edge of the electrode by shifting the location of the maximum stress and changing its magnitude. Generally, a reduced stress concentration in a separator could be realized

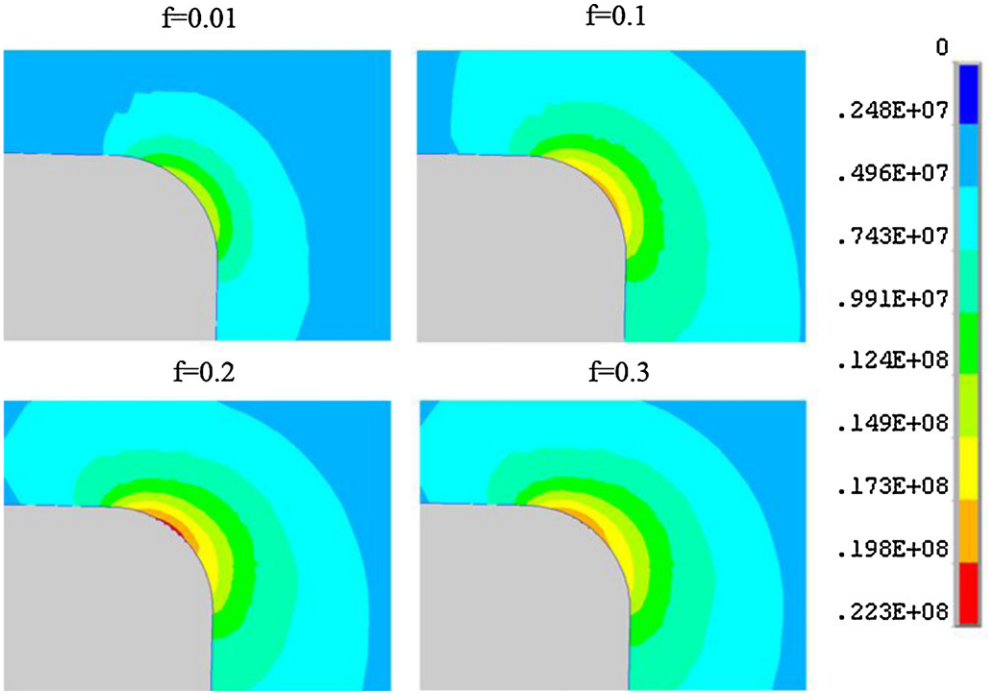

Fig. 10. Von Mises stress [Pa] in the corner under different friction conditions. Increased effective friction coefficient shifted the position of the high stress area.

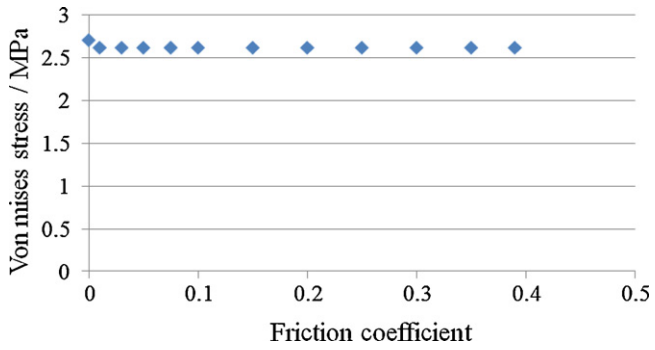

Fig. 11. Von Mises stress in the stable area of the separator.

Table 4
Three pairs of particle radius.

	Pair1 (r10)[a] (μm)	Pair2 (r50) (μm)	Pair3 (r90) (μm)
Anode	8.4	11.5	16
Cathode	2.45	3.35	4.65

[a] The definition of r10 is: the equivalent radius of 10% of the electrode particles is smaller than this value [39]. The definition of r50 and r90 can be derived similarly.

by reducing or softening the interactions between the separator and its surrounding electrodes.

5.4.2. Particle radius

Particle radius is an important factor that researchers are interested in. It has been shown that smaller particle radii reduces the lithium concentration gradient and lowers the hydrostatic stresses inside the active particle [7,13]. However, the influence of particle radii on the overall deformation of the electrode and the separator is not known.

In this part of the study, three pairs of anode and cathode particle radii were used to perform the analysis. These values correspond to r10, r50, and r90 particle radius in Ref. [37–39], as shown in Table 4. While the particle radius was altered, the volume fraction of the active material was kept the same for both electrodes.

Fig. 12 presents the SOC through the thickness of the electrode for both the anode and cathode at the end of a charging period obtained with different particle radii. As shown, the particle radius could change the average cross-section lithium concentration. For the anode, larger anodic particle radii resulted in smaller lithium concentration gradients, while the cathodic particle radii could only change the absolute values of the concentration. Larger cathodic particle radii resulted in greater concentration gradients, while

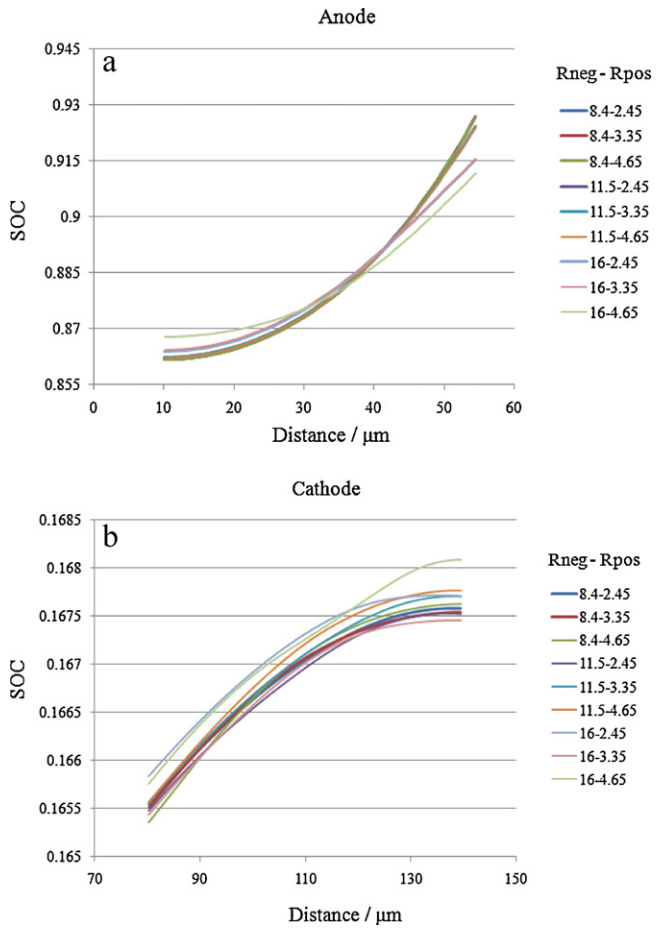

Fig. 12. SOC along the thickness of (a) anode and (b) cathode at the end of a charging period with different combinations of particle radii.

larger anodic particle radii reduced could the concentration gradient.

Fig. 13 presents the maximum Von Mises stress of the separator under differing particle radii. As shown, the maximum Von Mises stress was maintained around 15.5 MPa regardless of the particle radius. This can be explained by the fact that even though the lithium concentration along the thickness changed with the particle radius, the overall changes in both electrodes were very small. Taking the anode as an example, large particle radii (16 μm for the anode and 4.65 μm for the cathode) could increase the concentra-

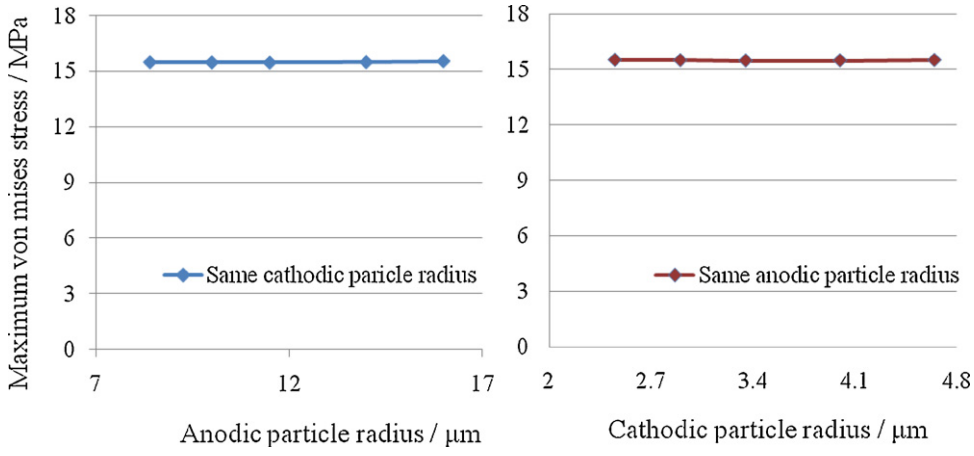

Fig. 13. Maximum Von Mises stress in the separator at the end of a charging period with different combinations of particle radii.

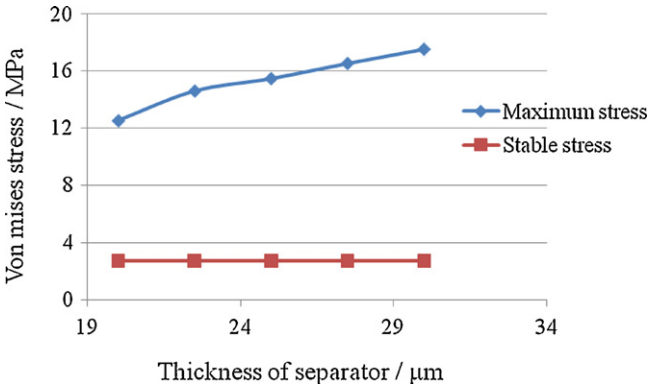

Fig. 14. Von Mises stresses in the separator with different thicknesses.

tion in the area close to the collector up to 1.2%, but also decreased the concentration in the area close to the separator by the same percentage. Therefore, the average concentration in the whole anode changed only slightly.

In conclusion, with the same volume fractions of active materials for both electrodes and under the same temperature variation, the particle radius did not yield any noticeable effect on the maximum stress of the separator. It should be noted that, in reality, smaller particles are often preferred due to better rate performance and decreased lithium gradient induced hydrostatic stresses inside the particles [7,13].

5.4.3. Separator thickness

A thin separator is desirable in order to reduce the internal resistance and improve the power and energy density of the battery [22]. However, the abuse tolerance concern must also be addressed. The thicker the separator is, the greater the mechanical strength and the lower the probability of puncture penetrations. The most widely used thickness for the separator of lithium ion batteries ranges from 20 μm to 30 μm.

As shown in Fig. 14, in the range of 20–30 μm, the maximum Von Mises stress in the separator near the electrode edge increased while the stress in the stable stress area slightly decreased with increasing the separator thickness. This suggests that a thinner separator would be subjected to a lower maximum stress during cell operation. Nevertheless, it should be noted that thinner thickness could also bring in lower mechanical strength and higher probability of puncture penetrations. Thus, thinner thickness does not necessarily decrease the chance of failure.

Parallel to this study, the viscoelastic behavior of polymeric separator in a battery environment and its modeling is under investigation [40]. In future work, a time, temperature dependent constitutive model for separator will be incorporated in the model for stress analysis of the separator.

6. Summary and conclusion

A macro-scale 2D 1.5-cell model was developed to evaluate stresses in the separator of a pouch cell. Coupled with previously developed multi-physics models, three groups of phenomena occurring inside the battery cell, namely electrochemical, thermal, and mechanical phenomena, were considered. Lithium diffusion induced and thermally induced stresses in the separator were investigated.

In the macro-scale 2D model, the electrodes and the separator were treated as homogenized media. The porous electrodes were considered as composites of electrode particles in an electrolyte matrix, and their effective properties were computed using the rule of mixtures.

It was demonstrated that the maximum stress in the separator always emerged at the inner side of the separator where it wrapped around the electrode edge when the lithium ion battery was fully charged, and the rest of the separator was in a relatively low and stable stress state. Thermal effects were demonstrated to be significant. The simulations revealed that although the thermal expansion increased the average strains in the electrodes and the separator, the local maximum stress and strain in the separator actually decreased with rising temperature.

Three groups of design adjustable parameters were studied at the same fully charged state. The results showed that the maximum Von Mises stress increased with increasing the thickness of the separator and the effective frictions between the separator and its adjacent electrodes. Under the same volume fractions of active materials, the particle radii had a negligible effect on the stress in the separator.

Acknowledgment

This research is supported by General Motors Company under a research contract ND4306101-LT442 and by NSF CMMI 1030821.

References

[1] M.D. Farrington, Journal of Power Sources 96 (2001) 260–265.
[2] C. Daniel, JOM 60 (9) (2008), http://www.tms.org/pubs/journals/jom/0809/.daniel-0809.html.
[3] M. Doyle, T.F. Fuller, J. Newman, Journal of the Electrochemical Society 140 (1993) 1526–1533.
[4] M. Doyle, J. Newman, A.S. Gozdz, C.N. Schmutz, J.M. Tarascon, Journal of the Electrochemical Society 143 (1996) 1890–1903.
[5] J. Christensen, J. Newman, Journal of the Electrochemical Society 153 (2006) A1019–A1030.
[6] J. Christensen, J. Newman, Journal of Solid State Electrochemistry 10 (2006) 293–319.
[7] X.C. Zhang, W. Shyy, A.M. Sastry, Journal of the Electrochemical Society 154 (2007) A910–A916.
[8] Y.T. Cheng, M.W. Verbrugge, Journal of Power Sources 190 (2009) 453–460.
[9] Y.T. Cheng, M.W. Verbrugge, Journal of Applied Physics 104 (2008) 083521.
[10] M.W. Verbrugge, Y.T. Cheng, Journal of the Electrochemical Society 156 (2009) A927–A937.
[11] S. Renganathan, G. Sikha, S. Santhanagopalan, R.E. White, Journal of the Electrochemical Society 157 (2) (2010) A155–A163.
[12] S. Golmon, K. Maute, M.L. Dunn, Computers and Structures 87 (2009) 1567–1579.
[13] R.E. Garcia, Y.M. Chiang, W.C. Carter, P. Limthongkul, C. M, Bishop 152 (2005) A255–A263.
[14] X. Xiao, W. Wu, X. Huang, Journal of Power Sources 195 (2010) 7649–7660.
[15] D. Bernardi, E. Pawlikowski, J. Newman, Journal of the Electrochemical Society 132 (1985) 5.
[16] X.C. Zhang, A.M. Sastry, W. Shyy, Journal of the Electrochemical Society 155 (7) (2008) A542–A552.
[17] V. Srinivasan, C.Y. Wang, Journal of the Electrochemical Society 150 (1) (2003) A98–A106.
[18] K.E. Thomas, J. Newman, Journal of the Electrochemical Society 150 (2) (2003) A176–A192.
[19] W. Wu, X. Xiao, D.H. Shi, IMECE2010-37870, Proceedings of the ASME2010 Congress, Vancouver, 2010.
[20] M. Alamgir, Presentation at the 26th International Battery Seminar & Exhibit, Fort Lauderdale, FL, March 16–19, 2009.
[21] P. Arora, Z.M. Zhang, Chemical Reviews 104 (2004) 4419–4462.
[22] J.O. Besenhard, Handbook of Battery Materials, Wiley-VCH, New York, 1999.
[23] S.S. Zhang, Journal of Power Sources 164 (2007) 351–364.
[24] X. Huang, Journal of Solid State Electrochemistry 15 (2011) 649–662.
[25] D.D. Domenico, A. Stefanopoulou, G. Fiengo, Journal of Dynamic Systems, Measurement, and Control 132 (2010 November) 061302.
[26] K.E. Thomas, C. Bogatu, J. Newman, Journal of the Electrochemical Society 148 (6) (2001) A570–A575.
[27] K. Kumaresan, G. Sikha, R.E. White, Journal of the Electrochemical Society 155 (2) (2008) A164–A171.
[28] S.A. Hallaj, R. Venkatachalapathy, J. Prakash, J.R. Selman, Journal of the Electrochemical Society 147 (7) (2000) 2432–2436.
[29] COMSOL, Rechargeable Lithium-Ion Battery, Version 3.5, 2009.
[30] L. Gaines, R. Cuenca, This report is available on the web at http://www.transportation.anl.gov/pdfs/TA/149.pdf.
[31] K.K. Chawla, Composite Materials Science and Engineering, Springer-Verlag, New York, 1987.

[32] W.D. Callister, Materials Science and Engineering: An Introduction, 5th ed., John Wiley & Sons, New York, 1999.
[33] S.J. Harris, A. Timmons, D.R. Baker, C. Monroe, Chemical Physics Letters 485 (2010) 265–274.
[34] R. Spotnitz, J. Franklin, Journal of Power Sources 113 (2003) 81–100.
[35] http://batteryuniversity.com/index.php/learn/article/charging_lithium_ion_batteries.
[36] D.E. Dieter, Mechanical Metallurgy, 3rd ed., Mc-Graw-Hill Publishing Company, New York, 1986.
[37] http://www.timcal.com/scopi/group/timcal/timcal.nsf.
[38] http://www.todaamerica.com/products/products.html.
[39] http://www.lactose.com/particle_size/d10_d50_d90.html.
[40] A. Sheidaei, X. Xiao, J. Wang, X. Huang, SAE 2011-PFL-168, Detroit MI, April, 2011.